Structural investigation and optical characteristics of low-energy hydrogen beam irradiated polyvinyl alcohol/polyaniline composite materials

Rabab K. Sendi[1] · A. Atta[2] · Nuha Al-Harbi[1] · Mohamed Rabia[3,4] · M. M. Abdelhamied[5]

Abstract

This work is demonstrate the optical characteristics of PVA/PANI composites using a homemade ion source for applied in optoelectronic devices. A solution casting technique was employed to fabricate the Polyvinyl Alcohol/Polyaniline (PVA/PANI) samples. The PVA/PANI samples are irradiated by hydrogen beam fluence of 5×10^{16}, 10×10^{16}, and 15×10^{16} ions/cm^2, respectively. The structural modifications of the PVA/PANI samples resulting from ion exposure are investigated by X-ray diffraction (XRD) and infrared spectroscopy (FTIR). The scanning microscope (SEM) is illustrate the morphology changes of the pure and irradiated samples. The optical gap of PVA/PANI was obtained by Tauc's formula. By enhancing ion dose from 5×10^{16} ions/cm^2 to 15×10^{16} ions/cm^2, the band gap of the PVA/PANI composite decreased from 2.89 eV to 2.71 eV, and the absorption edge moved of 2.43 eV to 1.45 eV. Furthermore, the number of carbon clusters increased from 57 to 66, while the band tail widened from 2.31 eV to 2.47 eV. In addition, other optical characteristics as the refractive indices and dielectric constant were computed. Moreover, Wemple/Di-Domenico analysis was employed to predict the dispersion measures of both untreated and ion-exposed samples. The results indicated that films exposed to 15×10^{16} ions/cm^2 are optimal for optical device applications.

Keywords Structural properties · Optical properties · Ion irradiation · Polymeric composite

1 Introduction

Recently, polymer composites have garnered significant interest in device fabrication because of their unique features, including ease of handling, compactness, versatility, simplicity of processing, cost-effectiveness, and strong mechanical properties (Atta et al. 2022). Composite materials have substantial potential such as LED devices, mobile phones, photovoltaic panels, detectors, TV sets, microelectromechanical systems, and immunity to electromagnetic interference (Alotaibi et al. 2022a; Abdellah, et al. 2021). This is primarily because of their distinctive optoelectronic characteristics, ease of preparation, low cost, and excellent durability (Mohamed et al. 2022).

Extended author information available on the last page of the article

The polyaniline (PANI) is exhibits a high absorption coefficient, making it suitable for use in the visible spectrum (Iqubal 2022). In addition, PANI offers non-linear optical (NLO) advantages, characterized by rapid responses, consistent electrical conductivity, and resistance to UV radiation (Ashour et al. 2021). Despite its superior properties, polyaniline (PANI) has low solubility, fusibility, and mechanical properties (Alotaibi et al. 2022b). Consequently, numerous efforts have been made to address these challenges by developing composite materials using polymers and biopolymers (Sadeghi and Farbodi 2018). Moreover, Polyvinyl alcohol (PVA), a stabilizer, is an excellent polymer for creating polyaniline/polymer nanocomposites (Nawas Mumthas et al. 2021; Wang et al. 2017). This is because of its high chemical reactivity, polarity, solubility in water, outstanding mechanical strength, and low cytotoxicity (Wang et al. 2020; Pattabi et al. 2007). Additionally, PVA imparts unique optical qualities to composites, such as retardation, light filtration, and polarization, owing to its excellent visibility and charge storage capability (Ferrández-Rives et al. 2017). PVA also facilitates polymer composite preparation via hydrogen bonding (El-Sayed et al. 2015).

The distinctive characteristics of the composite PVA/PANI, including as simple fabrications, shape variety, flexibility, and cost effectiveness, are attracting a lot of attention for applied in optical devices (Kaur et al. 2022). The insertion of conductive polymer (PANI) in the polymer matrix (PVA) is allowed their employment in a variety of high-tech devices and increases their potential applications (Aziz et al. 2021). In addition, a composite with excellent optical characteristics for optoelectronic applications has been developed by combining PVA with conductive PANI (Brza et al. 2021). In order to increase the composite efficiency for usage in optical instruments, the current research focuses on incorporating conductive PANI into a PVA matrix. Furthermore, PVA/PANI has certain properties that make it more effective in solar and optoelectronic devices. These features include low toxicity, high surface activity, and environmental friendliness (Abdeltwab and Atta 2021).

Ion irradiation exposure has gained attention recently due to its convenient use as a methodology for treating optoelectronic compounds (Shoaib et al. 2022). The optical behaviour of polymer nanocomposites is modified by subjecting them to ion beam exposure (Alfi et al. 2022). Ion irradiation improves polymer composites by cross-linking, free radical oxidation, and carbonization (Derkowska et al. 2001; Mongwaketsi et al. 2012). By depositing energy within the film structure, ion beam irradiation permanently alters its characteristics, resulting in an improvement in optical behavior (Abd-Elnaiem et al. 2022; Abdel Reheem et al. 2016). The modifications of ion irradiation is influenced by ion energy, and beam intensity of the ion bombardment (Abdeltwab et al. 2022). Using SRIM/TRIM software (Ziegler et al. 2010a), the range of ions striking PVA/PANI were evaluated. The energy loss of recoiling atoms within the polymer composite films were determined with SRIM/TRIM (Donya and Salah 2020).

This work aimed to fabricate PVA/PANI films using the cast solution technique. The novelty of this work is using of low-energy ion source to activate surface characteristics of the manufactured films for improving the optical characteristics of the PVA/PANI composite. Moreover, the films were exposed to varying fluencies of hydrogen beams using of low-energy ion source with relatively wide beam width and not heat the samples. Subsequently. XRD, FTIR, and SEM were performed to examine the structural and surface properties of PVA/PANI films. In addition conductivity and other optical parameters were calculated. Based on these findings, the irradiated PVA/PANI films can be utilized in optoelectronic

applications. The results show that PVA/PANI optical characteristics have been significantly altered, enabling their employment in a variety of super capacitor devices.

2 Experimental work

Hydrochloric acid (40%AR) and Ammonium peroxide sulfate (98.7% AR), Aniline $C_6H_5NH_2$ (94 g/mol) received from Oxford Lab Chemistry. The dimethylformamide (DMF) and polyvinyl alcohol (Mw = 17,900, DP = 1580, 97.6%) were supplied respectively from Sigma-Aldrich and Elgoumhouria Co., Egypt. PVA/PANI films were synthesized using a casting solution preparation technique described in the literature (Abdelhamied et al. 2020, 2021, 2022). The synthesized films were then exposed to H ion beams with various fluences (5×10^{16}, 10×10^{16}, and 15×10^{16} ions/cm^2) using a homemade cold-cathode ion source. As illustrated in Fig. 1, which discussed previously (Al-Muntaser et al. 2022), this cold-cathode ion source featured for gas entry into the chamber and surrounded by a magnet. Electrons were released at the cathode and traversed the chamber towards the anode, colliding with the gas molecules to generate plasma. The operational parameters of the ion source included a density of 170 µA/cm, pressure of 2.2×10^{-4} mbar, and energy 5 keV. The SRIM/TRIM method was used to calculate the ion range in PVA/PANI (Ziegler et al. 2010b).

The characteristics of PVA were determined using XRD (XRD, XRD-6000) with $\lambda = 1.5406$ Å in 2θ range of 4° to 90°. The structure of the films were examined using FTIR (ATI Mattson, Genesis series, Unicam, UK) in wavelength of 400 to 4000 cm^{-1}. The morphology of the films were analyzed by (SEM, JEOL, Japan). The films were sputtered with a layer gold at 32 mA for 25 s before scanning and measuring. The double-beam JascoV-670 UV/VIS is evaluate the absorption and reflection spectra of the untreated and exposed films over the wavelength of 190 to 1050 nm at room temperature. Ion diffusion into a depth of 1 µm is achieved by SRIM simulations, allowing one to better comprehend ion-target interactions. The stopping power and beam depth were calculated by the SRIM simulation code. These measurements are the result of an interaction between a 5 keV hydrogen ion and a PVA/PANI blend. The SRIM model uses fast calculations to examine ion concentrations and distributions.
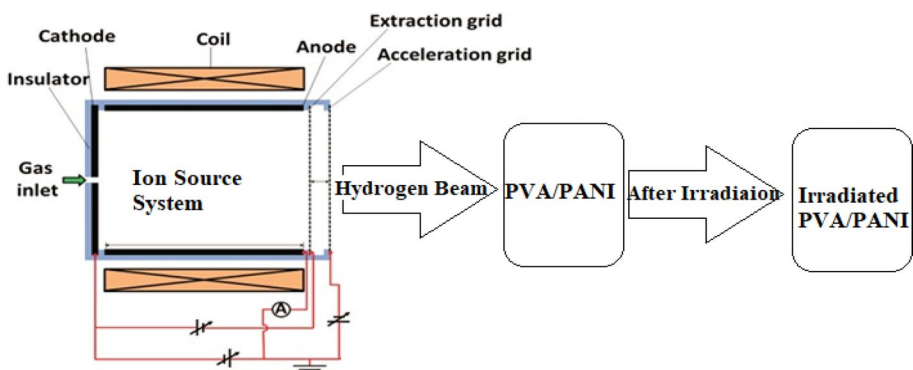

Fig. 1 The ion source with electrical circuit

3 Results and discussion

SRIM simulations were employed to investigate ion densities and distributions, as shown in Fig. 2. The images were generated using data obtained by 5 keV hydrogen beam interactions in a 1 μm thick PVA/PANI sample. Figure 2a shows the ion distribution within penetration of 1134 Å. In Fig. 2b, a tree-like pattern of collisional hydrogen ions was observed, with implantation up to 1 μm into the PVA/PANI. The ionization resulting from the incident and recoiling atoms is shown in Fig. 2c. When comparing the effects of ionization caused by penetrating hydrogen ions, the latter were negligible. Figure 2d shows the atom distributions on the target by hydrogen ions (Lee et al. 2018). Due to their light mass, hydrogen atoms generate more vacancies than other targeted atoms.

The XRD of the unirradiated and hydrogen ion beam exposed PVA/PANI films at various fluence are shown in Fig. 3. The PVA film exhibits significant peak located at ~ 20.1° which is assigned to the plane (101) for PVA matrix. Moreover, this pattern also holds a small hump located at ~ 40.8, which confirms the semicrystalline structure for the prepared PVA film. The figure also demonstrates that the PVA/PANI film exhibited a structure near to PVA, thus confirming the amorphous behavior of PANI (Atta et al. 2021). Moreover, the introduction of PANI resulted in a decrease in peak intensity, confirming a reduction in crystallinity.

Additionally, the identifiable diffraction peaks remained consistent after the exposure of the PVA/PANI films to the ion beam. Consequently, there was a significant difference in the peak intensities, which gradually decreased by irradiation, indicating a decrease in the crystalline phase. This are to molecular chain cross-linking, which transformed the organized crystal structure into a disordered structure by forming connections between
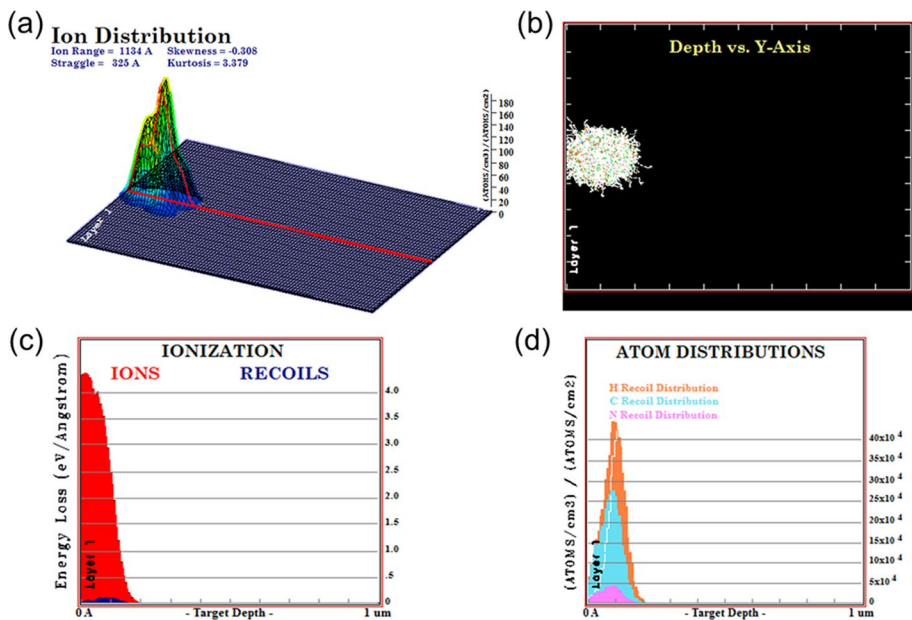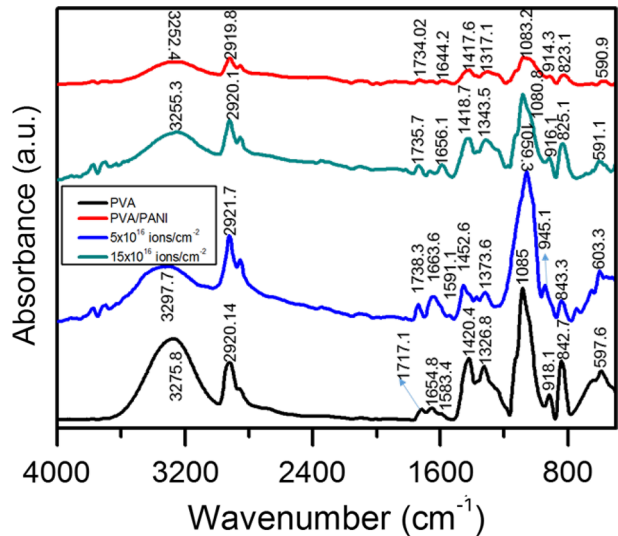

Fig. 2 **a** Ion distribution, **b** ion depth, **c** ionization, and **d** atom distributions of 5 keV hydrogen ion beam interacting with PVA/PANI

Fig. 3 XRD of PVA, non-treated, and treated PVA/PANI films
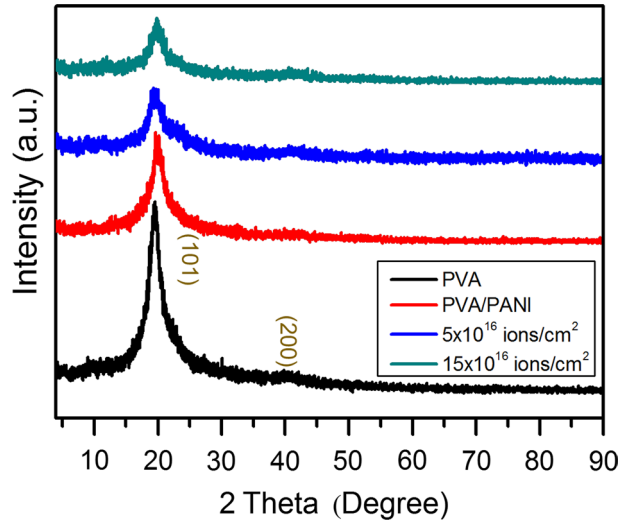
**Fig. 4** FTIR of PVA, the non-treated and treated PVA/PANI films

neighboring chains (Abdel-Galil et al. 2020a). The decrease in crystallization of the PVA/PANI films after ion beam exposure suggested strong interactions between the films and ion beams.

For confirmation, FTIR is reveal the functional groups of PVA, PVA/PANI, and irradiated PVA/PANI films, as in Fig. 4. In case of the PVA, a broad band was observed at 3276 cm^{-1}, corresponding to the hydroxyl vibration group. Additionally, band 2920 cm^{-1} is to CH_2 (Korbag and Mohamed Saleh 2016). A peak of 1717 cm^{-1} is to C=O vibration, resulting from oxidation during preparation and processing. Additional characteristic peak is 1655 cm^{-1} (associated with water absorption), 1420.4 cm^{-1} (indicating CH_2 bending), 1326.8 cm^{-1} (related to coupling of O–H with C–H wagging vibrations), 918.1 cm^{-1} (reflecting CH_2 rocking), and 842.7 cm^{-1} (representing C–C stretching) (Jipa et al. 2012).

Furthermore, two peaks were observed at 1146.3 cm^{-1}, attributed to the shoulder stretching of C–O and the crystalline sequence of PVA, whereas the band at 1085 cm^{-1} showed C–O stretching, OH bending, and the amorphous nature of PVA (Asran et al. 2010). After the incorporation of PANI, a new peak was observed at 746.5 cm^{-1} (Deshkulkarni et al. 2018). Additionally, changes in peak position and intensity were observed, confirming the interaction between the PVA and PANI. These results indicated the successful preparation of PVA/PANI composite films. For irradiated PVA/PANI films, the peaks decreased, indicating a decrease in the number of OH groups. This suggested a weakening of hydrogen bonding and free radical creation, leading to the escape of H gases (Mirershadi et al. 2016). Moreover, most peak positions shifted after irradiation (Derkowska et al. 2007).

The PVA morphology is shown in Fig. 5a, revealing a homogeneous surface without punctures. Additionally, Fig. 5b shows SEM micrographs of the PVA film after incorporating PANI, indicating the formation of granules and the expansion of white observations, suggesting the growth of PANI within the polymer matrices. The surface morphologies of the irradiated PVA/PANI films by H-ion beam are shown in Fig. 5c, d. Noticeable differences in surface properties were observed upon exposure to ions without surface defects. Moreover, the roughness of the films rapidly increased because of the interactions resulted in the heating and evaporation of particles across the interaction region (El-Saftawy et al. 2014).
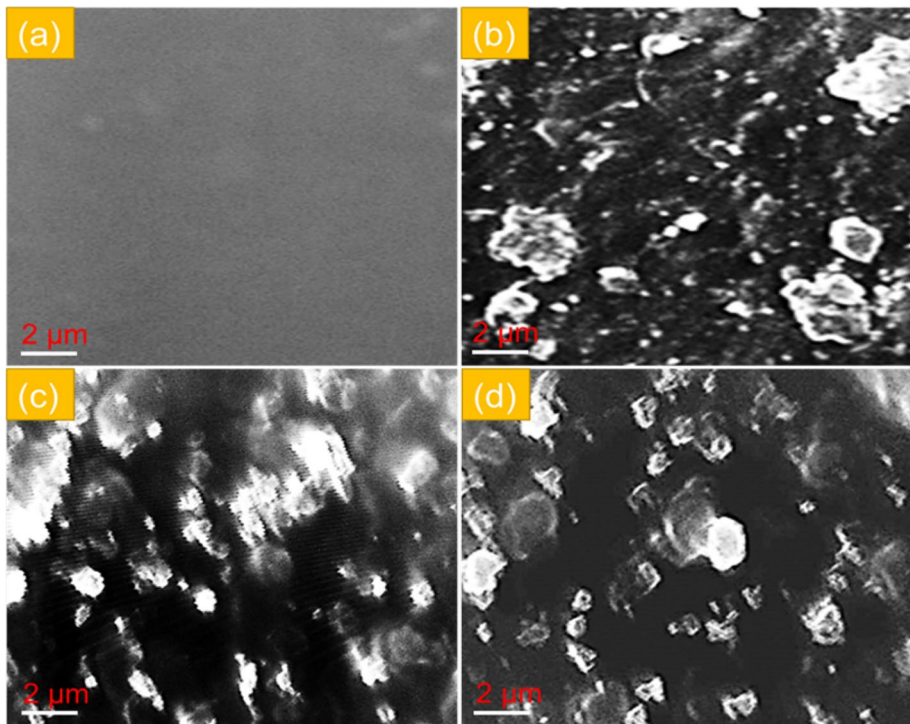
Fig. 5 SEM micrographs of **a** PVA film, **b** the non-treated PVA/PANI, **c** the exposed PVA/PANI film by 5×10^{16} ions/cm^2, and **d** the exposed PVA/PANI film by 15×10^{15} ions/cm.^{2}

Figure 6a illustrates the absorption of untreated PVA/PANI films and those exposed to hydrogen ion beams with fluences of 5×10^{16}, 10×10^{16}, and 15×10^{16} ions/cm^2. It is evident that the films exposed to ions exhibited behaviors similar to those of the untreated film. However, with increasing irradiation, the absorbance increased (Ali et al. 2009). Moreover, the coefficient (α) was derived by Rao et al. (2012); Chintala et al. 2016):

$$\alpha = \frac{2.303A}{d} \tag{1}$$

The α for are plotted with photon energy (hν) in Fig. 6b. As the ion fluence increased from 5×10^{16} ions/cm^2 to 15×10^{16} ions/cm^2, a clear redshift of the absorption edge energy is noticed from 2.43 eV to 1.45 eV. An increase in the ion beam effect resulted in a higher absorbance coefficient for the untreated film. This shift might be attributed to an increase in defect creation and prevalence. The Tauc's equation (Abdel-Galil et al. 2020b) is used to determine the energy gap (E$_g$).

$$\alpha h\nu = A\left(h\nu - \mathrm{E}_g\right)^m \tag{2}$$

The energy of incoming photons ($h\nu$) was determined by calculating $h\nu = 1240/\lambda$, where (λ) represents the wavelength, A is a fixed value which is called the band tailing factor (Tauc parameter) (Hassanien and Radaf 2023; Hassanien et al. 2023a), E$_g$ signifies band gap, (m) is electronic transition type, which take 1/2 for direct and for indirect (m = 2). So, the relationship among ($\alpha h\nu)^{1/2}$ against photon energy can be used to determine the indirect
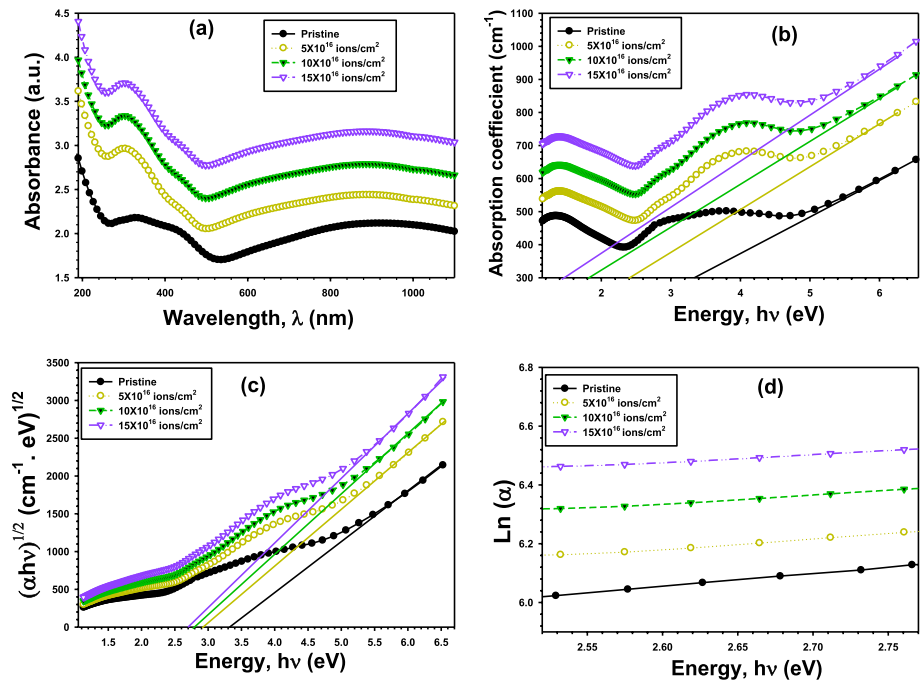

Fig. 6 **a** Absorbance A with λ, **b** Absorption coefficient α with hν, **c** ($\alpha h\nu)^{1/2}$ with hν, and **d** Ln(α) with hν, of untreated and treated PVA/PANI films

band gap of both the untreated and subjected films (El-Denglawey et al. 2022; Sharma et al. 2022). Figure 6c and the corresponding values in Table 1 are obtained by extending the straight-line segments of the graphs to zero absorption values. By increasing irradiation fluence of 5×10^{16} to 15×10^{16} ions/cm^2, the indirect band gap will reduce from 2.89 eV to 2.71 eV. The defects inside the band gap are created due to the interactions between the ion beams with nanocomposite layer (Banerjee and Kumar 2011).

In the insufficient energy region, known as the Urbach's tail region, the transition occurred among localized tail levels and broadened band states. The absorption coefficients (α), given by Zaki et al. (2017):

$$\alpha(\nu) = \alpha_o \, e^{h\nu/E_u} \tag{3}$$

(α_o) is a fixed value and E_u represents the band tail (Urbach tail), which indicates the extent of the localization of states within the band gap energy. Thus, the band tails of the untreated and treated films were determined by plotting $\ln(\alpha)$ against the photon energies, as in Fig. 6d. The inverse of the slopes of the linear portions of these graphs was used to calculate the band tails of all films, as shown in Table 1. These method to determine the band tails is used by other literatures (Hassanien 2022; Hassanien and Sharma 2019). The calculated Urbach tail of the PVA/PANI film is 1.95 eV and rises to 2.31 eV, 2.39 eV, and 2.47 eV following exposure to 5, 10, and 15×10^{16} ions/cm^2, correspondingly. These behavior has been observed for other composites (Evingür and Pekcan 2018). The increase in Urbach tail values upon the exposure to ion beam is attributed to the defects which is presented in polymer matrix after irradiation. Adding graphene oxide (GO) to PVC is creates a more disordered nanocomposite, which in turn raises the Urbach tail energy E_u (Taha and Saleh 2018). Besides, the carbonaceous cluster is extracted using the following expression (57):

$$N = \left(\frac{34.4}{E_g} \right)^2 \tag{4}$$

where N refers to the number of carbons in cluster. From Table 1, it is found that N value of the pure film increase after irradiation, which is attributed to that the irradiation by ion beam leads to dehydrogenation processes, increasing the carbons concentration, therefore the cluster sizes.

The reflectance (R) of pure and exposed samples was plotted against the wavelengths of incoming light ranging from 200 to 1050 nm, as shown in Fig. 7a. The reflectance decreased as the wavelength increased and leveled off at longer wavelengths for the untreated and exposed films. In addition, radiation exposure increased the reflectance

Table 1 Absorption edge, E_g and E_U of pure and exposed PVA/PANI films

	Absorption edge (nm)	Indirect band gap ($E_{g(ind)}$) (eV)	Urbach tail (E_U) (eV)	Carbon clusters (N)
PVA/PANI	3.39 ± 0.25	3.38 ± 0.24	1.95 ± 0.20	55 ± 0.4
5×10^{16} ions/cm^2	2.43 ± 0.22	2.89 ± 0.16	2.31 ± 0.18	57 ± 0.5
10×10^{16} ions/cm^2	1.86 ± 0.15	2.81 ± 0.12	2.39 ± 0.15	60 ± 0.8
15×10^{16} ions/cm^2	1.45 ± 0.20	2.71 ± 0.24	2.47 ± 0.16	66 ± 0.6
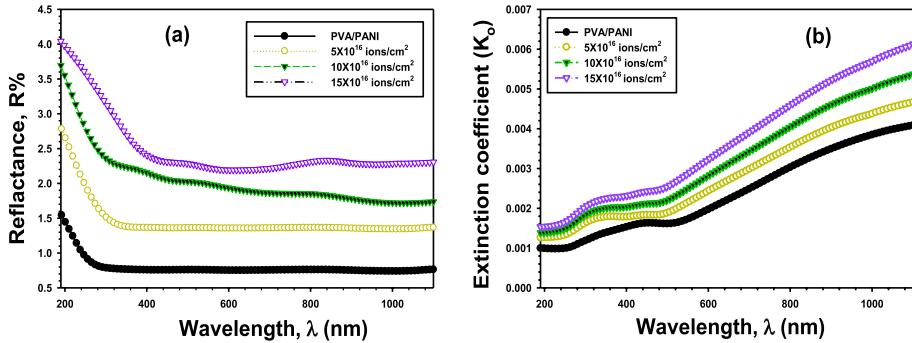
Fig. 7 **a** R with λ, **b** K_o with λ for pure and treated PVA/PANI films. The refractive index (n) is given by the Fresnel's formula (Iliopoulos et al. 2012)

of the pristine film, indicating a reduction in light scattering. This suggested that the exposed films became less chaotic over time. The extent of light loss due to scattering could be determined using the extinction coefficient (K_o) by employing the following formula (Kakil et al. 2018):

$$K_o = \frac{\alpha \lambda}{4\pi} \tag{5}$$

Figure 7b illustrates the effect of varying the ion beam energies on the extinction coefficients as a function of the incoming photon wavelengths for both the untreated and exposed PVA/PANI films. As the density of the flaws and, consequently, the absorption coefficients increased in the exposed films, the extinction coefficients (K_o) also increased.

$$n = \frac{(1 + R)}{(1 - R)} + \sqrt{\frac{4R}{(1 - R)^2} - K_o^2} \tag{6}$$

Figure 8a shows that the index (n) of untreated and exposed PVA/PANI composite films changed with the wavelength. Both pristine and exposed films exhibited the expected dispersion behavior, with the refractive index decreasing as the wavelength increase. However, after exposure to the hydrogen beams, the pristine films exhibited a gradual enhancement in the refractive index. This increase could be attributed to the promotion of covalent bond formation across different chains by the free radicals generated during ion irradiation (Albe and Moller 1996; Nouh et al. 2020). The increase in the refractive index might also be influenced by the creation of defects, which lead to the randomized breaking of bonds. Additionally, the refractive indices below the absorption edges displayed irregular dispersion behaviors in pristine and exposed films (Farag and Yahia 2010). The band gap of the irradiated films changes as additional homopolar connections and defects formed. The conductivity (σ_{opt}) represents the electrical conductivity resulting from the changes in the electric field. Using the absorption coefficient (α) as a reference, the optical conductivities of both the untreated and exposed films could be calculated using the following formula (Saadeddin et al. 2007; Hassouni et al. 2013):
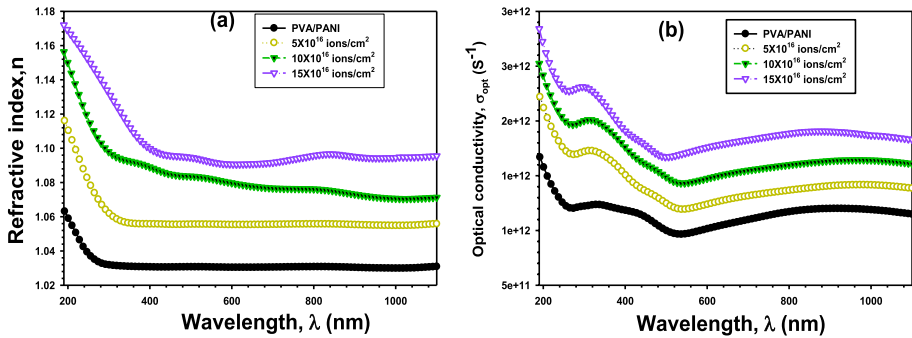
Fig. 8 **a** Refractive indices n, **b** σ_{opt} of pure and treated PVA/PANI films
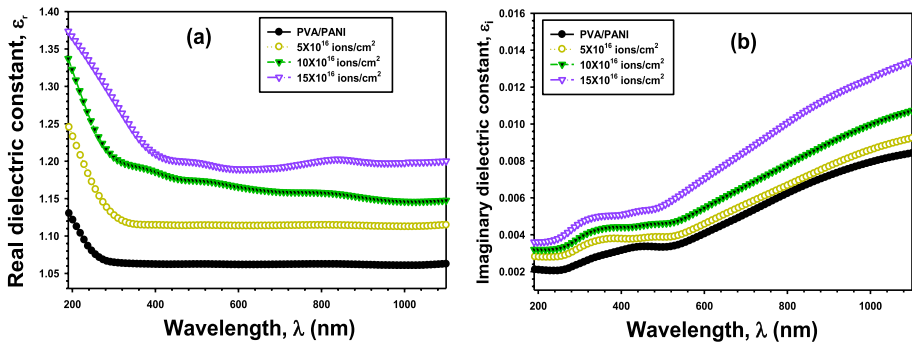

Fig. 9 **a** ε_r and **b** ε_i with λ of untreated and exposed PVA/PANI films

$$\sigma_{opt} = \frac{\alpha n c}{4\pi} \tag{7}$$

Figure 8b shows the wavelength dependence of the changes in the optical conductivities of both the untreated and exposed films. It could be observed that the absorption coefficients increased, this due to the changes in in the optical conductivity of the films (Mohamed and Abdel-Kader 2019).

Complex dielectric constants are among the most basic features of a substance and are composed of real and imaginary components, as described in the following formula (Donya et al. 2020):

$$\varepsilon = \varepsilon_r + i\varepsilon_i \tag{8}$$

ε_r reis deduced from the index (n) and coefficient (K_o) using formula (Abd El-Rahman et al. 2019):

$$\varepsilon_r = n^2 - K_o^2 \tag{9}$$

Figure 9a illustrates the variations in ε_r and relative permittivity with the wavelength (λ), for pure and exposed films. This index followed a trend like that of ε_r. As ion exposure enhanced, the ε_r levels of the untreated and treated films also increased. This is because the development of covalent connections between chains, leading to an increase

in photon energy loss (Rasheed et al. 2019). Furthermore, the next equation (Al-Hamdani et al. 2014) could be utilized to calculate the ε_i by.

$$\varepsilon_i = 2nK_o \tag{10}$$

Figure 9b shows the changes in ε_i with λ for both the pure and exposed samples. With increasing ion beams, the PVA/PANI film densities and refractive indices increased, causing an elevation in the characteristic ε_i of the pristine films.

Consequently, both the unaltered and exposed PVA/PANI films displayed typical dispersion behaviors for the refractive indices (n) in the transparent region ($\lambda > 400$ nm). Therefore, Wemple and DiDomenico's relationship (Alharbi and El-Rahman 2017) suggested modeling the refractive index using the single-oscillator paradigm:

$$\frac{1}{n^2 - 1} = \frac{E_O}{E_d} - \frac{1}{E_O E_d}(h\nu)^2 \tag{11}$$

E_o and E_d represent the single oscillator and dispersion energies (contributing to the transition strength between bands), respectively. Therefore, in Fig. 10a, the $(n^2-1)^{-1}$ and $(h\nu)^2$ is depicted for pure and exposed films. By examining the intercept and slope of the linear fit, we determined the E_o and Ed values. Additionally, by extrapolating the vertical portion of each curve to an ordinate value of $(h\nu)^2 = 0$ (Al-Zahrani et al. 2015), we estimated the stationary refractive indices of the unaltered and exposed films.
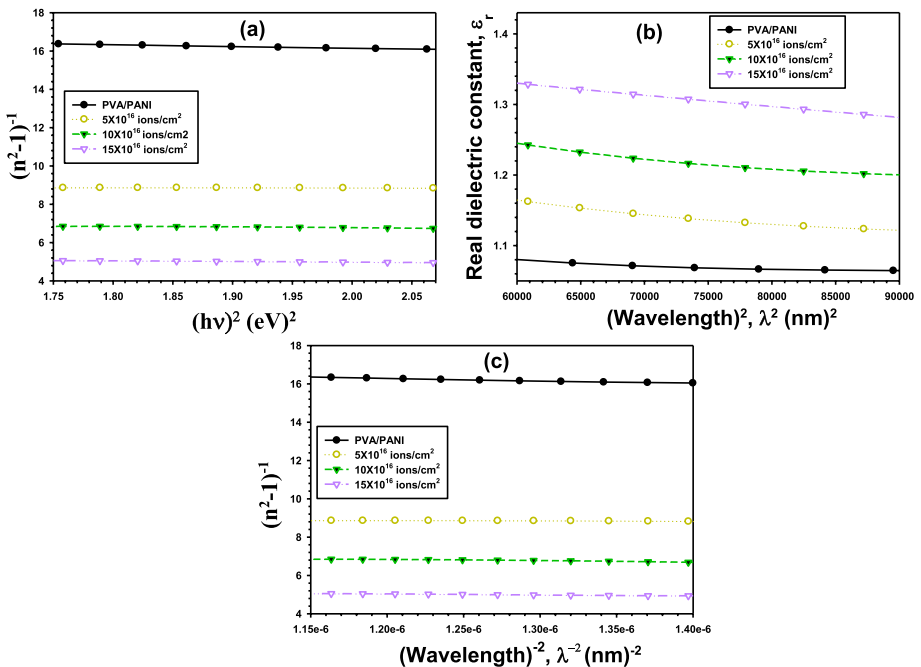
Fig. 10 **a** $(n^2-1)^{-1}$ wirh $(h\upsilon)^2$, **b** ε_r with λ^2, and **c** $(n^2-1)^{-1}$ with λ^{-2} for pure and treated films

$$n_o = \left(1 + \frac{E_d}{E_O}\right)^{1/2} \tag{12}$$

Therefore, we used this formula to determine the dielectric constants at zero frequency for the pure and exposed films. Table 2 presents the measured values of E_o, E_d, and both unexposed and exposed PVA/PANI films. Exposure by 5×10^{16}, 10×10^{16}, and 15×10^{16} ions/cm^2 led to shifting in E_o from 3.98 eV to 4.04 eV, 4.20 eV, and 4.13 eV, correspondingly. The E_o is empirically correlated to the E_g, in which $E_o \sim 1.5\ E_g$ as concluded by Wemple and DiDominico (El-Nahass et al. 2009a). For the finding results, it can be observed that $E_o = 1.17\ E_g$, 1.39 E_g, 1.49 E_g, and 1.52 E_g of the pure and bombarded films by 5×10^{16} ions/cm^2, 10×10^{16} ions/cm^2, and 15×10^{16} ions/cm^2, correspondingly. Additional variables, namely, the lattice constant (ε_l) and the ratio between the concentrations of free carriers and their effective mass (N/m*), were calculated according to El-Nahass et al. 2009b:

$$\varepsilon_r = \varepsilon_l - \left(\frac{e^2}{4\pi^2\varepsilon_s c^2}\frac{N}{m^*}\right)\lambda^2 \tag{13}$$

where (c) represents the speed of light, (e) represents the electron charge, and (ε_s) represents the dielectric constant of empty space. Figure 10b illustrates the relationship between the real dielectric and λ^2 at longer wavelengths for pure and exposed films. The ε_l and N/m* values of the unexposed and exposed films are listed in Table 2. In addition, we calculated the plasma resonant frequencies (W_p) for each valence electron participating in the transition using the formula (Hassanien et al. 2022):

$$W_p = \frac{e^2}{\varepsilon_o} \times \frac{N}{m^*} \tag{14}$$

After exposure to different ion beam impacts, the pure films exhibited consistent increases in ε_l and N/m*. These increases could be attributed to the differences in the bond lengths at varying radiation exposure levels. Fortunately the interaction of PVA/PANI with the hydrogen beam after irradiation results in an increase in W_p. Moreover, XRD data show that the production of free radicals is responsible for the observed variations in Wp with irradiation.

The untreated PVA/PANI films, as well as the exposed films, had refractive indices (n) at longer wavelengths, moderate oscillatory wavelengths (λ_o), and oscillator length intensity (S_o). The refractive index results were analyzed using a one-term Sellmeier oscillator, as presented below (Hassanien et al. 2023b):

Table 2 n_o, ε_∞, E_d, E_o, ε_l, and N/m* of untreated and exposed PVA/PANI films

	n_o	ε_∞	E_d (eV)	E_o (eV)	ε_l	N/m* $\times$ 10^{39}kg^{-1} m^{-3}
PVA/PANI	1.02 ± 0.15	1.06 ± 0.14	0.24 ± 0.03	3.98 ± 0.30	1.08 ± 0.10	0.88 ± 0.02
5×10^{16} ions/cm^2	1.05 ± 0.12	1.11 ± 0.11	0.46 ± 0.02	4.04 ± 0.27	1.16 ± 0.09	1.65 ± 0.04
10×10^{16} ions/cm^2	1.07 ± 0.08	1.14 ± 0.09	0.61 ± 0.05	4.20 ± 0.18	1.24 ± 0.11	1.87 ± 0.05
15×10^{16} ions/cm^2	1.09 ± 0.10	1.19 ± 0.06	0.81 ± 0.04	4. 13 ± 0.24	1.33 ± 0.12	2.02 ± 0.07

$$(n_\infty^2 - 1)/(n^2 - 1) = 1 - \left(\frac{\lambda_o}{\lambda}\right)^2 \tag{15}$$

Figure 10c illustrates the $(n^2-1)^{-1}$ and λ^{-2} for both the unexposed and exposed samples at long wavelengths. The n_∞ and λ_o calculated by subtracting the intercept of the linear segment from its slope, as in Table 3. The S_o is given by Hassanien and Sharma (2020):

$$S_o = (n_\infty^2 - 1)/(\lambda_o)^2 \tag{16}$$

Both n_∞ and S increased with increasing ion beam impact. In contrast, the λ_o rates decreased when the films were exposed to light.

The next formula was used to estimate non-linear optical (NLO) responses (Hassanien and Sharma 2021):

$$P = X^{(1)}E + X^{(2)}E^2 + X^{(3)}E^3 \tag{17}$$

P refers to polarization, and $X^{(1)}$, $X^{(2)}$, and $X^{(3)}$ are the 1st, 2nd, and 3rd NLO susceptibilities, respectively. The $X^{(1)}$ and $X^{(3)}$ are given by the following equations (Kaur et al. 2020):

$$X^{(1)} = \frac{\left(n^2 - 1\right)}{4\pi} \tag{18}$$

$$X^{(3)} = A\left(X^{(1)}\right)^4 \tag{19}$$

A is a fixed value of 1.7×10^{-10} for $\chi^{(3)}$ in esu, where the refractive indices are given by the following equation:

$$n(\lambda) = n_o(\lambda) + n_2\left(E^2\right) \tag{20}$$

n_o and n_2 are the refractive linear and NLO, respectively, calculated using the following equation (Sakhno et al. 2020):

$$n_2 = \frac{12\pi X^{(3)}}{n_o} \tag{21}$$

The variations in $X^{(1)}$ and $X^{(3)}$ against λ for the pristine and exposed films are shown in Fig. 11a, b, respectively. The quantities $X^{(1)}$ and $X^{(3)}$ increased with an increase in the exposure dose, indicating an increase in the local polarizability of the defect centers as the ion fluence increased. In addition, Fig. 11c illustrates the non-linear refractive index fluctuation. Following the same trend as $X^{(3)}$, n_2 enhanced with ion fluence. Based on these

Table 3 W_p, n_∞, λ_o and S_o, of untreated and exposed PVA/PANI films

	$W_p \times 10^{13}$ (Hz)	n_∞	λ_o (nm)	$S_o \times 10^{11}$ (m^{-2})
PVA/PANI	0.26	1.03	268	8.3
5×10^{16} ions/cm^2	0.48	1.05	198	2.8
10×10^{16} ions/cm^2	0.52	1.07	321	14.4
15×10^{16} ions/cm^2	0.59	1.10	342	16.2
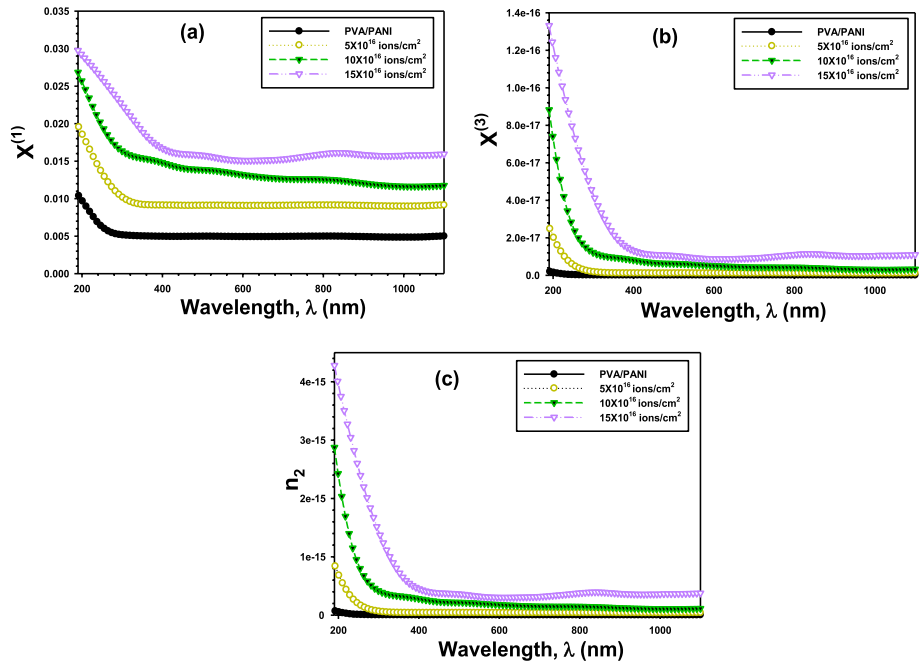
Fig. 11 **a** $X^{(1)}$, **b** $X^{(3)}$, and **c** n_2 versus λ of pure and exposed PVA/PANI films

findings, irradiated PVA/PANI films are preferred over untreated films for non-linear optical applications.

4 Conclusion

In this study, an easy and novel approach was devised for utilizing irradiated nanocomposite films in optical systems. These irradiation composites have unparalleled surface and optical properties compared to those of traditional materials. PVA/PANI films were successfully fabricated using the cast solution technique, as shown by the XRD and FTIR analyses. The samples were subjected to various hydrogen beam fluencies. SEM imaging revealed changes in the morphological characteristics of the film surfaces after the ion exposure. It has been hypothesized that the development of defects and the chain session procedure are to blame for the morphological modifications observed in PVA/PANI. The optical band gap of the untreated film reduced as the ion beam fluence increased. Furthermore, upon irradiation, the absorption edge shifted from 3.37 eV for PVA/PANI to 2.42, 1.84, and 1.45 eV, respectively, with increasing ion fluence to 5×10^{16}, 10×10^{16}, and 15×10^{16} ions/cm^2. In optical systems, non-linear properties are crucial, especially for photonics integrated devices. Nonlinear optical parameter research is of critical importance in optoelectronics. These findings indicated that irradiation with PVA/PANI enhanced its surface properties, making it highly suitable for various applications. These results support the notion that hydrogen beam irradiation technology is more suitable for energy-related applications. This research showed that irradiated PVA/PANI composite materials can exhibit

novel, emergent characteristics and different usefulness through the use of straightforward, customizable procedures. The results of this research are going to be utilized the irradiated PVA/PANI composite for use in a variety of optical device applications.

Data availability The datasets generated during and/or analysed during the current study are available from the corresponding author on reasonable request.

Declarations

Conflicts of interest The authors declare no conflict of interest.

Competing interests The authors have no relevant financial.

Ethics approval Not applicable (The Research is not involving the studies on human or their data).

Consent to participate Consent to participate.

Consent for publication Consent for publication.

References

Abd El-Rahman, M., Yassien, K.M., Yassene, A.A.: Effect of gamma irradiation on the optical properties of epoxy resin thin films. Optik **183**, 962–970 (2019)

Abdel Reheem, A., Ahmed, M., Abdelhamid, M., Ashour, A.: Verification of high efficient broad beam cold cathode ion source. Rev. Sci. Instrum. **87**, 083302–083308 (2016)

Abdel-Galil, A., Atta, A., Balboul, M.: Effect of low-energy oxygen ion beam treatment on the structural and physical properties of ZnO thin films. Surf. Rev. Lett. **27**, 1–13 (2020a)

Abdel-Galil, A., Assiri, M., Yahia, I.: Optical analysis of methyl violet thin films/polymeric substrate for flexible organic technology. Opt. Quantum Electron. **52**, 1–20 (2020b)

Abdelhamied, M., Atta, A., Abdelreheem, A., Farag, A., El Okr, M.: Synthesis and optical properties of PVA/PANI/Ag nanocomposite films. J. Mater. Sci. Mater. Electron. **31**, 22629–22641 (2020)

Abdelhamied, M.M., Atta, A., Abdelreheem, A.M., Farag, A.T.M., El Sherbiny, M.A.: Oxygen ion induced variations in the structural and linear/nonlinear optical properties of the PVA/PANI/Ag nanocomposite film. Inorg. Chem. Commun. **133**, 108926–108937 (2021)

Abdelhamied, M.M., Abdelreheem, A.M., Atta, A.: Influence of ion beam and silver nanoparticles on dielectric properties of flexible PVA/PANI polymer composite films. Plast. Rubber Compos. **51**(1), 1–12 (2022)

Abdellah, M.Y., et al.: A novel and highly effective natural vibration modal analysis to predict nominal strength of open hole glass fiber reinforced polymer composites structure. Polymers **13**(8), 1201–1220 (2021)

Abd-Elnaiem, A.M., Salman, O.S., Hakamy, A., Hussein, S.I.: Mechanical characteristics and thermal stability of hybrid epoxy and acrylic polymer coating/nanoclay of various thicknesses. J. Inorg. Organomet. Polym. Mater. **32**(6), 2094–2102 (2022)

Abdeltwab, E., Atta, A.: Structural and electrical properties of irradiated flexible ZnO/PVA nanocomposite films. Surf. Innov. **40**, 1–9 (2021)

Abdeltwab, E., Atta, A., Bek, A.: Structural, mechanical and electrical properties of sputter-coated copper thin films on polyethylene terephthalate. Int. J. Mod. Phys. B **36**(20), 2250125–2250135 (2022)

Albe, K., Moller, W.: Radiation effects and defects in solids: incorporating plasma science and plasma technology. Radiat. Eff. Defects Solids **141**, 85–97 (1996)

Alfi, A.A., Abumelha, H.M., Qurban, J., Alnoman, R.B., Alaysuy, O., Bayazeed, A., El-Metwaly, N.M.: Preparation of microfibrillated cellulose/polyvinyl alcohol test strip integrated with novel chemosensor for colorimetric determination of diisopropyl fluorophosphate. Polym. Compos. **43**(8), 5364–5374 (2022)

Al-Hamdani, N.A., Al-Alawy, R.D., Hassan, S.J.: Effect of gamma irradiation on the structural and optical properties of ZnO thin films. IOSR J Comput Eng **16**, 11–16 (2014)

Alharbi, S., El-Rahman, K.: Gamma irradiation effects on the linear and nonlinear optical properties of non-crystalline Sb_2S_3 films. Chalcog. Lett. **14**, 529–537 (2017)

Ali, Z., Ali, F., Hosam, A.: Effect of electron beam irradiation on the structural properties of PVA/V_2O_5 xerogel. Spectrochim. Acta Part A Mol. Biomol. Spectrosc. **72**, 868–875 (2009)

Al-Muntaser, A.A., Pashameah, R.A., Sharma, K., Alzahrani, E., Tarabiah, A.E.: Reinforcement of structural, optical, electrical, and dielectric characteristics of CMC/PVA based on GNP/ZnO hybrid nanofiller: nanocomposites materials for energy-storage applications. Int. J. Energy Res. **46**(15), 23984–23995 (2022)

Alotaibi, B.M., Al-Yousef, H.A., Alsaif, N.A., Atta, A.: Characterization and optical properties of polymer nanocomposite films for optoelectronic applications. Surf. Innov. **40**, 109904–109914 (2022a)

Alotaibi, B.M., Al-Yousef, H.A., Alsaif, N.A., Atta, A.: Oxygen beam induced modifications on the structural characteristics and physico-chemical properties of PANI/lead sulfide composite films. Inorg. Chem. Commun. **144**, 109904–109914 (2022b)

Al-Zahrani, J., El-Hagary, M., El-Taher, A.: Gamma irradiation induced effects on optical properties and single oscillator parameters of Fe-doped CdS diluted magnetic semiconductors thin films. Mater. Sci. Semicond. Process. **39**, 74–78 (2015)

Ashour, G., Hussein, M., Sobahi, T.: Nanocomposite containing polyamide and GNS for enhanced properties. Synth. Charact. J. Umm Al-Qura Univ. Appl. Sci. **7**(1), 1–6 (2021)

Asran, A.S., Henning, S., Michler, G.H.: Polyvinyl alcohol–collagen–hydroxyapatite biocomposite nanofibrous scaffold: mimicking the key features of natural bone at the nanoscale level. Polymer **51**(4), 868–876 (2010)

Atta, A., Abdelhamied, M.M., Abdelreheem, A.M., Berber, M.R.: Flexible methyl cellulose/polyaniline/silver composite films with enhanced linear and nonlinear optical properties. Polymers **13**, 1225 (2021)

Atta, A., Abdelhamied, M.M., Essam, D., Shaban, M., Alshammari, A.H., Rabia, M.: Structural and physical properties of polyaniline/silver oxide/silver nanocomposite electrode for supercapacitor applications. Int. J. Energy Res. **46**(5), 6702–6710 (2022)

Aziz, S.B., Asnawi, A.S., Abdulwahid, R.T., Ghareeb, H.O., Alshehri, S.M., Ahamad, T., Kadir, M.F.Z.: Design of potassium ion conducting PVA based polymer electrolyte with improved ion transport properties for EDLC device application. J. Mater. Res. Technol. **13**, 1225–1241 (2021)

Banerjee, S., Kumar, A.: Swift heavy ion irradiation induced modifications in the optical band gap and Urbach's tail in polyaniline nanofibers. Nucl. Instrum. Methods Phys. Res. Sect. B **269**, 2798–2806 (2011)

Brza, M.A., Aziz, S.B., Anuar, H., Alshehri, S.M., Ali, F., Ahamad, T., Hadi, J.M.: Characteristics of a plasticized PVA-based polymer electrolyte membrane and h^+ conductor for an electrical double-layer capacitor: structural, morphological, and ion transport properties. Membranes **11**(4), 296–317 (2021)

Chintala, K.M., Panchal, S., Rana, P., Chauhan, R.: Structural, optical and electrical properties of gamma-rays exposed selenium nanowires. J. Mater. Sci. Mater. Electron. **27**, 8087–8093 (2016)

Derkowska, B., Mulatier, J.C., Fuks, I., Sahraoui, B., Phu, X.N., Andraud, C.: Third-order optical nonlinearities in new octopolar molecules and their dipolar subunits. JOSA B **18**(5), 610–616 (2001)

Derkowska, B., Wojdyła, M., Bała, W., Jaworowicz, K., Karpierz, M., Grote, J.G., Sahraoui, B.: Influence of different peripheral substituents on the nonlinear optical properties of cobalt phthalocyanine core. J. Appl. Phys. **101**(8), 083112–081128 (2007)

Deshkulkarni, B., Viannie, L.R., Ganachari, S.V., Banapurmath, N.R., Shettar, A.: Humidity sensing using polyaniline/polyvinyl alcohol nanocomposite blend. In: IOP Conference Series: Mater. Sci. Eng. **376**, 012063 (2018)

Donya, H., Salah, A.: Effect of 60 keV argon ion implantation in Makrofol® DE 1–1 on the optical properties. Polym. Bull. **77**, 6349–6375 (2020)

Donya, H., Taha, T., Alruwaili, A., Tomsah, I., Ibrahim, M.: Micro-structure and optical spectroscopy of PVA/iron oxide polymer nanocomposites. J. Mater. Res. **9**, 9189–9194 (2020)

El-Denglawey, A., Aly, K.A., Dahshan, A., Hassanien, A.S.: Optical characteristics of thermally evaporated thin a-$(Cu_2ZnGe)_{50-x}Se_{50+x}$ films. ECS J. Solid State Sci. Technol. **11**(4), 044006–0440010 (2022)

El-Nahass, M., Farag, A., Abd-El-Salam, F.: Effect of gamma irradiation on the optical properties of nano-crystalline InP thin films. Appl. Surf. Sci. **255**, 9439–9443 (2009a)

El-Nahass, M.M., Farag, A.A.M., Abd-El-Salam, F.: Effect of gamma irradiation on the optical properties of nano-crystalline InP thin films. Appl. Surf. Sci. **255**(23), 9439–9443 (2009b)

El-Saftawy, A., Abd El Aal, S., Badawy, Z., Soliman, B.: Investigating wettability and optical properties of PADC polymer irradiated by low energy Ar ions. Surf. Coat. Technol. **253**, 249–254 (2014)

El-Sayed, S., Abel-Baset, T., Abou Elfadl, A., Hassen, A.: Effect of nanosilica on optical, electric modulus and AC conductivity of polyvinyl alcohol/polyaniline films. Phys. B Condens. Matter **464**, 17–27 (2015)

Evingür, G.A., Pekcan, Ö.: Optical energy band gap of PAAm-GO composites. Compos. Struct. **183**, 212–215 (2018)

Farag, A., Yahia, I.: Structural, absorption and optical dispersion characteristics of rhodamine B thin films prepared by drop casting technique. Opt. Commun. **283**, 4310–4317 (2010)

Ferrández-Rives, M., Beltrán-Osuna, Á.A., Gómez-Tejedor, J.A., Gomez Ribelles, J.L.: Electrospun PVA/bentonite nanocomposites mats for drug delivery. Materials **10**, 1448–1465 (2017)

Hassanien, A.S.: Intensive linear and nonlinear optical studies of thermally evaporated amorphous thin Cu–Ge–Se–Te films. J. Noncryst. Solids **586**, 121563 (2022)

Hassanien, A.S., El-Radaf, I.M.: Effect of fluorine doping on the structural, optical, and electrical properties of spray deposited Sb_2O_3 thin films. Mater. Sci. Semicond. Process. **160**, 107405–107415 (2023)

Hassanien, A.S., Sharma, I.: Band-gap engineering, conduction and valence band positions of thermally evaporated amorphous $Ge_{15-x}Sb_xSe_{50}Te_{35}$ thin films: influences of Sb upon some optical characterizations and physical parameters. J. Alloys Compd. **798**, 750–763 (2019)

Hassanien, A.S., Sharma, I.: Optical properties of quaternary a-$Ge15_{-x}Sb_xSe_{50}Te_{35}$ thermally evaporated thin-films: refractive index dispersion and single oscillator parameters. Optik **200**, 163415 (2020)

Hassanien, A.S., Sharma, I.: Dielectric properties, optoelectrical parameters and electronic polarizability of thermally evaporated a-Pb–Se–Ge thin films. Phys. B **622**, 413330 (2021)

Hassanien, A.S., Aly, K.A., Elsaeedy, H.I., Alqahtani, A.: Optical characterization and dispersion discussions of the novel thermally evaporated thin a-$S_{50-x}Ge_{10}Cd_xTe_{40}$ films. Appl. Phys. A **128**(11), 1021 (2022)

Hassanien, A.S., Sharma, I., Sharma, P.: Optical and dispersion studies of thin $S_{35-x}Ge_{15}Sn_xTe_{50}$ films: assessment of some physical parameters of samples. Phys. Scr. **98**(4), 045911 (2023a)

Hassanien, A.S., Sharma, I., Sharma, P.: Inference of Sn addition on optical properties of the novel thermally evaporated thin a-$Ge_{15}Te_{50}S_{35-x}Sn_x$ films and some physical properties of their glasses. Mater. Chem. Phys. **293**, 126887 (2023b)

Hassouni, M.H., Mishjil, K.A., Chiad, S.S., Habubi, N.F.: Effect of gamma irradiation on the optical properties of Mg doped CdO Thin films deposited by spray pyrolysis. Int. Lett. Chem. Phys. Astron. **11**, 26–37 (2013)

Iliopoulos, K., El-Ghayoury, A., Derkowska, B., Ranganathan, A., Batail, P., Gindre, D., Sahraoui, B.: Effect of the counter cation on the third order nonlinearity in anionic Au dithiolene complexes. Appl. Phys. Lett. **101**(26), 261105–261109 (2012)

Iqubal, S.M.: Characterization, surface morphology and microstructure of water soluble colloidal MnO_2 nanoflakes. J. Umm Al-Qura Univ. Appl. Sci. **8**, 1–4 (2022)

Jipa, I.M., Stoica, A., Stroescu, M., Dobre, L.M., Dobre, T., Jinga, S., Tardei, C.: Potassium sorbate release from poly (vinyl alcohol)-bacterial cellulose films. Chem. Pap. **66**(2), 138–143 (2012)

Kakil, S.A., Sabr, B.N., Hana, L.S., Abbas, T.A.-H., Hussin, S.Y.: Effects of a low dose of gamma radiation on the morphology, and the optical and the electrical properties of an ITO thin film as an electrode for solar cell applications. J. Korean Phys. Soc. **72**, 561–569 (2018)

Kaur, R., Singh, K., Tripathi, S.: Study of linear and nonlinear optical responses of $MoSe_2$–PMMA nanocomposites. J. Mater. Sci. Mater. Electron. **31**, 19974–19988O (2020)

Kaur, R., Singh, K.P., Tripathi, S.K.: Electrical, linear and non-linear optical properties of $MoSe_2$/PVA nanocomposites as charge trapping elements for memory device applications. J. Alloys Compd. **905**, 164103–164113 (2022)

Korbag, I., Mohamed Saleh, S.: Studies on the formation of intermolecular interactions and structural characterization of polyvinyl alcohol/lignin film. Int. J. Environ. Stud. **73**(2), 226–235 (2016)

Lee, S., Byeon, E., Jung, S., Kim, D.G.: Heterogeneity of hard skin layer in wrinkled PDMS surface fabricated by Ar ion-beam irradiation. Sci. Rep. **8**(1), 1–8 (2018)

Mirershadi, S., Ahmadi-Kandjani, S., Zawadzka, A., Rouhbakhsh, H., Sahraoui, B.: Third order nonlinear optical properties of organometal halide perovskite by means of the Z-scan technique. Chem. Phys. Lett. **647**, 7–13 (2016)

Mohamed, M.B., Abdel-Kader, M.: Effect of excess oxygen content within different nano-oxide additives on the structural and optical properties of PVA/PEG blend. Appl. Phys. A **125**, 209–220 (2019)

Mohamed, A.M., Alamri, H.R., Hamad, M.A.: Investigation on giant electrocaloric properties in ferroelectric polymer P (VDF-TrFE)(65/35). Russ. J. Phys. Chem. A **96**(10), 2259–2264 (2022)

Mongwaketsi, N., Khamlich, S., Pranaitis, M., Sahraoui, B., Khammar, F., Garab, G., Maaza, M.: Physical origin of third order non-linear optical response of porphyrin nanorods. Mater. Chem. Phys. **134**(2–3), 646–650 (2012)

Nawas Mumthas, I.N., Mohamad Noh, M.F., Arzaee, N.A., Mohamed, N.A., Mohd Nasir, S.N.F., Alessa, H., Mat Teridi, M.A.: Improving the stability and efficiency of polymer solar cells by γ-radiated graphitic carbon nitride. Int. J. Energy Res. **45**(10), 15284–15297 (2021)

Nouh, S., Benthami, K., Samy, R., El-Hagg, A.: Effect of gamma radiation on the structure and optical properties of polycarbonate-polybutylene terephthalate/silver nanocomposite films. Chem. Phys. Lett. **741**, 137123–137128 (2020)

Pattabi, M., Amma, B.S., Manzoor, K.: Photoluminescence study of PVP capped CdS nanoparticles embedded in PVA matrix. Mater. Res. Bull. **42**, 828–835 (2007)

Rao, C.V.S., Ravi, M., Raja, V., Bhargav, P.B., Sharma, A.K., Rao, V.N.: Preparation and characterization of PVP-based polymer electrolytes for solid-state battery applications. Iran. Polym. J. **21**, 531–536 (2012)

Rasheed, H.S., Abbas, I.A., Kadhum, A.J., Maged H.C.: The effect of gamma irradiation on the optical properties of (PVA-PAA-Al2O3) films. In: AIP Conference Proceedings, pp. 020013, AIP Publishing LLC (2019)

Saadeddin, I., Pecquenard, B., Manaud, J.P., Decourt, R., Labrugère, C., Buffeteau, T., Campet, G.: Synthesis and characterization of single-and co-doped SnO_2 thin films for optoelectronic applications. Appl. Surf. Sci. **253**(12), 5240–5249 (2007)

Sadeghi, A.K., Farbodi, M.: Preparation of polyaniline-polyvinyl alcohol-silver nanocomposite and characterization of its mechanical and antibacterial properties. Sci. Eng. Compos. Mater. **25**, 975–982 (2018)

Sakhno, O., Yezhov, P., Hryn, V., Rudenko, V., Smirnova, T.: Optical and nonlinear properties of photonic polymer nanocomposites and holographic gratings modified with noble metal nanoparticles. Polymers **12**, 480–501 (2020)

Sharma, I., Sharma, P., Hassanien, A.S.: Optical properties and optoelectrical parameters of the quaternary chalcogenide amorphous $Ge_{15}Sn_xS_{35-x}Te_{50}$ films. J. Noncryst. Solids **590**, 12167–12173 (2022)

Shoaib, M., Jamshaid, H., Alshareef, M., Alharthi, F.A., Ali, M., Waqas, M.: Exploring the potential of alternate inorganic fibers for automotive composites. Polymers **14**(22), 4946–4961 (2022)

Taha, T., Saleh, A.: characterization of PVC/fGO polymer nanocomposites. Appl. Phys. A **124**, 1–12 (2018)

Wang, H., Wen, H., Hu, B., Fei, G., Shen, Y., Sun, L., Yang, D.: Facile approach to fabricate waterborne polyaniline nanocomposites with environmental benignity and high physical properties. Sci. Rep. **7**, 43694–43706 (2017)

Wang, J., Chi, H., Zhou, A., Zheng, R., Bai, H., Zhang, T.: Facile synthesis of multi-functional elastic polyaniline/polyvinyl alcohol composite gels by a solution assembly method. RSC Adv. **10**, 22019–22026 (2020)

Zaki, M., Ali, A.M., Amin, R.M.: Effect of gamma irradiation on optical and chemical properties of cellulose nitrate thin films. J. Adhes. Sci. Technol. **31**, 1314–1327 (2017)

Ziegler, J.F., Ziegler, M.D., Biersack, J.P.: SRIM–The stopping and range of ions in matter (2010). Nucl. Instrum. Methods Phys. Res. Sect. B **268**, 1818–1823 (2010a)

Ziegler, J.F., Ziegler, M.D., Biersack, J.P.: SRIM–The stopping and range of ions in matter (2010). Nucl. Instrum. Methods Phys. Res. Sect. B **268**(11–12), 1818–1823 (2010b)

Publisher's Note Springer Nature remains neutral with regard to jurisdictional claims in published maps and institutional affiliations.

Authors and Affiliations

Rabab K. Sendi[1] · A. Atta[2] · Nuha Al-Harbi[1] · Mohamed Rabia[3,4] · M. M. Abdelhamied[5]

✉ A. Atta
aamahmad@ju.edu.sa

Rabab K. Sendi
rksendi@uqu.edu.sa

Nuha Al-Harbi
nfhariby@uqu.edu.sa

Mohamed Rabia
mohamedchem@science.bsu.edu.eg

M. M. Abdelhamied
m_elbana52@yahoo.com

[1] Department of Physics, Faculty of Applied Sciences, Umm Al-Qura University, Makkah, Saudi Arabia

[2] Physics Department, College of Science, Jouf University, P.O. Box: 2014, Sakaka, Saudi Arabia

[3] Nanomaterials Science Research Laboratory, Chemistry Department, Faculty of Science, Beni Suef University, Beni Suef 62514, Egypt

[4] Nanophotonics and Applications Laboratory, Physics Department, Faculty of Science, Beni Suef University, Beni Suef 62514, Egypt

[5] Charged Particles Laboratory, Radiation Physics Department, National Center for Radiation Research and Technology (NCRRT), Egyptian Atomic Energy Authority (EAEA), Cairo, Egypt